Nuclear Instruments and Methods in Physics Research A 775 (2015) 154–161

Contents lists available at ScienceDirect

Nuclear Instruments and Methods in Physics Research A

journal homepage: www.elsevier.com/locate/nima

The dynamic time-over-threshold method for multi-channel APD based gamma-ray detectors

T. Orita [a,*], K. Shimazoe [b], H. Takahashi [b]

[a] Japan Atomic Energy Agency, Fukushima, Japan
[b] Department of Nuclear Management and Engineering, The University of Tokyo, Bunkyō, Japan

ARTICLE INFO

Article history:
Received 3 September 2014
Received in revised form
30 November 2014
Accepted 4 December 2014
Available online 13 December 2014

Keywords:
Gamma-ray detector
Avalanche photodiode
CMOS
ASIC
Time-over-threshold

ABSTRACT

t– Recent advances in manufacturing technology have enabled the use of multi-channel pixelated detectors in gamma-ray imaging applications. When obtaining gamma-ray measurements, it is important to obtain pulse height information in order to avoid unnecessary events such as scattering. However, as the number of channels increases, more electronics are needed to process each channel's signal, and the corresponding increases in circuit size and power consumption can result in practical problems. The time-over-threshold (ToT) method, which has recently become popular in the medical field, is a signal processing technique that can effectively avoid such problems. However, ToT suffers from poor linearity and its dynamic range is limited. We therefore propose a new ToT technique called the dynamic time-over-threshold (dToT) method [4]. A new signal processing system using dToT and CR-RC shaping demonstrated much better linearity than that of a conventional ToT. Using a test circuit with a new $Gd_3Al_2Ga_3O_{12}$ (GAGG) scintillator and an avalanche photodiode, the pulse height spectra of ^{137}Cs and ^{22}Na sources were measured with high linearity. Based on these results, we designed a new application-specific integrated circuit (ASIC) for this multi-channel dToT system, measured the spectra of a ^{22}Na source, and investigated the linearity of the system.

1. Introduction

Time-over-threshold (ToT) [1–3] is a pulse processing method in which an input pulse signal is compared with a preset threshold level in order to convert an input charge into a digital pulse with a corresponding time width. As it can be implemented without an independent analog-to-digital converter, The ToT method has advantages over conventional pulse height systems in terms of circuit integration and power consumption. Although ToT is attractive, the relation between input charge and time width of the output pulse is strongly non-linear [4,5]. To correct this, we propose a new dynamic time over threshold (dToT) [6] principle in which linearity can be significantly improved through the use of an independent pulse shaping section. In this article, we propose a combination CR-RC filter and dToT method that can achieve a high degree of linearity. Using charge sensitive amplifiers with constant current feedback resistors has been proposed as a means of improving ToT. [7] However, such systems cannot be used to implement shaping amplifiers; because their signal frequency responses are strongly dependent on pulse amplitude, the noise effect changes with pulse height, making them difficult to use for the processing of signals with wide dynamic range input charges. The dToT method, by contrast, is easily implementable and can be applied using an independent shaping amplifier.

2. Dynamic time-over-threshold method

2.1. The principle of dToT

The dToT method is a new ToT technique in which threshold voltage is not kept constant but is dynamically altered to catch up to the input signal after signal pulse detection. Some delay time is needed before sweeping the threshold voltage, and, together with the change in threshold voltage, this can be implemented using two mono-stable multi-vibrators. One of the vibrators responds to the rise of comparator output by producing a digital pulse with a fixed time width corresponding to the delay time, while the other responds to the falling edge of this digital pulse by producing another digital pulse that is shaped by an RC low-pass filter and sent to a comparator reference input.

* Corresponding author.
E-mail address: orita.tadashi@jaea.go.jp (T. Orita).

http://dx.doi.org/10.1016/j.nima.2014.12.014
0168-9002/

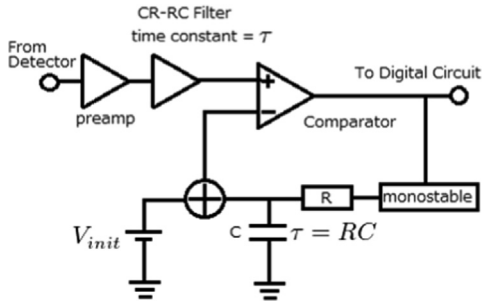

Fig. 1. Combination CR-RC filter and dToT system.

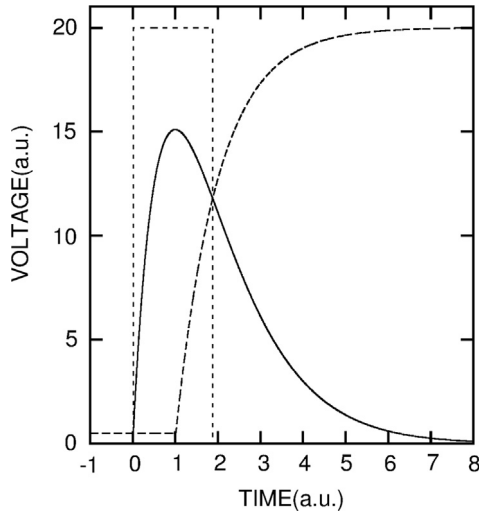

Fig. 2. Typical waveforms of CR-RC+dToT system, Solid line: Shaping output, Dashed line: Threshold, Dotted line: Comparator output. The time unit is normalized with τ.

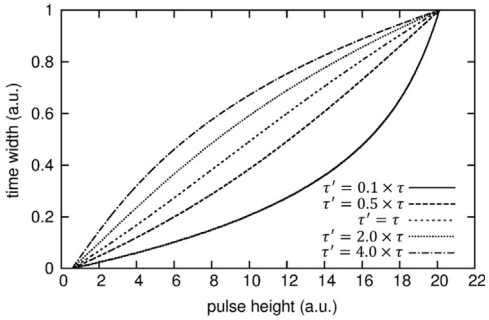

Fig. 3. Linearity of dToT system at different threshold voltage time constants (τ') for $\tau_d = \tau$. The time width unit is normalized in order to make the max time width 1.

2.2. Combining the CR-RC filter and dToT

Fig. 1 shows a combination CR-RC filter and dToT circuit; Fig. 2 shows typical transient waveforms produced in different stages of the system.

The CR-RC waveform f(t) is expressed as

$$f(t) = he^{1}\frac{t}{\tau}exp\left(-\frac{t}{\tau}\right) \quad (1)$$

where τ and h are the time constant and pulse height, respectively, of the CR-RC filter output. The RC filtered step signal $g(t)$ that is produced with some offset and delay can be written as

$$g(t) = (V_{DD} - V_{ini})\left\{1 - exp\left(-\frac{(t-\tau_d)}{\tau'}\right)\right\} + V_{ini} \quad (2)$$

where V_{DD} is the supply voltage, V_{ini} is the offset value for the initial threshold voltage, τ' is the time constant of the RC circuit, and τ_d is the delay time. Using arbitrary units and setting $\tau = 1$ and $V_{DD} = 20$, eqs. (1) and (2) were used to perform the calculations described in the rest of this article.

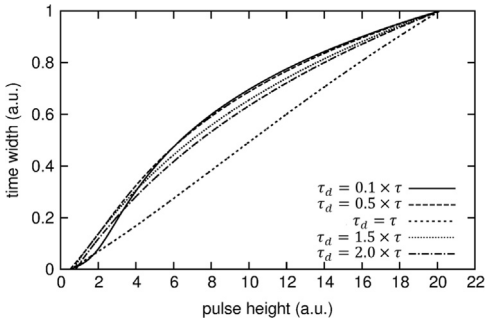

Fig. 4. Linearity of dToT system at different delay times (τ_d) for $\tau' = \tau$.

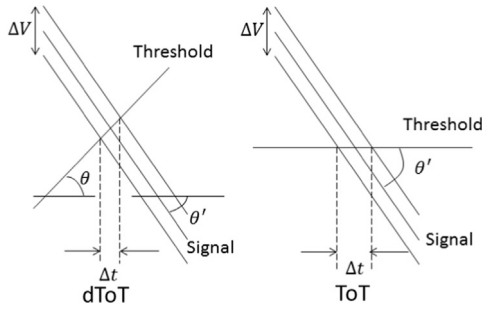

Fig. 5. Schematic definitions of time jitter and voltage noise for dToT and ToT, θ: Angle of threshold slope at the second crossing point, θ': Angle of the shaper signal slope at the second crossing point.

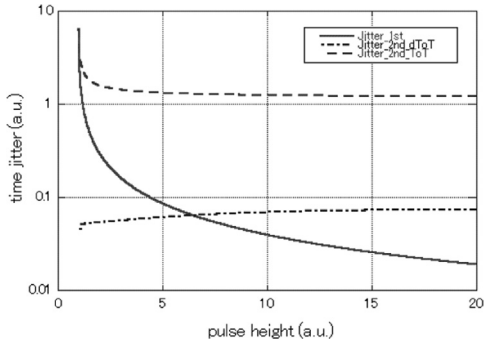

Fig. 6. Time jitters of dToT and ToT systems ($\tau = \tau' = \tau_d$, $V_{ini} = 1.0$), Solid line: Jitter at the first cross point, Dashed line: Jitter at the second cross point of ToT, Long dashed dotted line: Jitter at the second cross point of dToT.

2.3. Linearity

We analyzed the linearity of the dToT system as a function of the time constant of the dynamic threshold voltage (τ') with the delay time set to the time constant of the CR-RC filter (τ), as shown in Fig. 3. We also analyzed the dToT linearity as a function of the

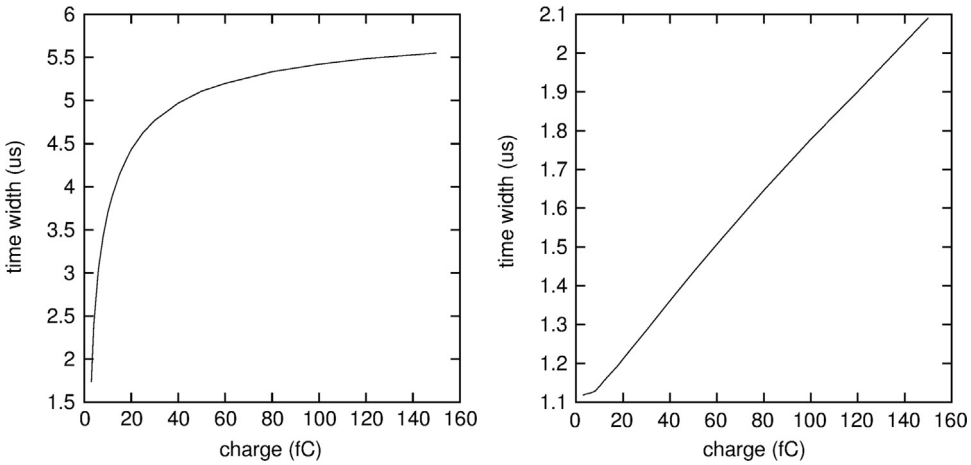

Fig. 7. ToT and dToT linearities of the prototype circuit, Left: ToT, Right: dToT, INL (ToT)=70.66%; INL (dToT)=2.7%.

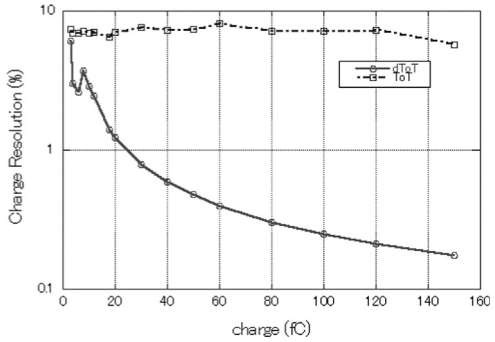

Fig. 8. Charge resolutions of dToT and ToT, Solid line: dToT; Dotted line: ToT.

delay time (τ_d) of the dynamic threshold voltage in order to determine the optimal time constant $\tau' = \tau$, as shown in Fig. 4. It is seen that non-linearity increases with difference between the time constants of the CR-RC filter and the dynamic threshold voltage; if these are equal, the linearity will be optimized at an integral non linearity (INL) of 1.6%. If the delay time does not match the time constant of the CR-RC filter, the linearity becomes poor.

2.4. Time jitter

The slopes of the input signal and the dynamic threshold voltage at the cross point are important, as voltage signal slope determines how voltage noise is converted into time jitter. The combined system shown in Fig. 2 is similar to a normal ToT at its first crossing point because its threshold voltage is constant prior to this crossing. Therefore, we investigated time jitters at the second crossing point for both a dToT and a ToT. Assuming that the voltage noise is ΔV and the time jitter is Δt, as shown in Fig. 5, the time jitter-to-voltage-noise ratio ($\Delta t/\Delta V$) can be written as follows:

$$\frac{\Delta t}{\Delta V} = \frac{\cos\theta \times \cos\theta'}{\sin(\theta+\theta')} \tag{3}$$

In a normal ToT, the threshold is constant ($\theta = 0$), and we can write the jitter-to-noise ratio as

$$\frac{\Delta t}{\Delta V} = \frac{1}{\tan\theta'} \tag{4}$$

The time jitters for the dToT and ToT at each pulse height voltage are plotted in Fig. 6. The time jitter at the first cross point is also added in Fig. 6 and its equation is the same as Eq. (4). But its θ' is an angle at the first crossing point.

As shown in the figure, the dToT method provides a lower value of $\Delta t/\Delta V$. This characteristic, along with its high linearity, results in lower jitter production using the dToT method.

3. Experimental results

3.1. Linearity and jitter

We implemented the dToT and ToT methods by constructing a prototype circuit with a CR-RC shaping filter (Fig. 7) and used a pulse generator (ORTEC 419) to investigate the linearity of the relationship between input charge and time width. In this prototype circuit, we used a charge sensitive amplifier module (Clear Pulse 5005 H) and a CR-RC filter with a time constant of 1 μs. At low input charges, the linearity of the circuit was reduced owing to reductions in signal-to-noise ratio (SNR) caused by the addition of noise from the pulse generator to the signal. However the measured linearity (INL=2.7%) of the dToT was much better than that of the normal ToT (INL=70.66%) using the same CR-RC filter. In order to measure jitter characteristics, we compared the charge resolution of each input charge with its time width distributions (Fig. 8), from which we were able to confirm that the dToT also had improved jitter characteristics and the effect of the jitter at the first cross point clearly appears in the lower charge area of dToT case. The linearities were evaluated using linear least square fitting in which the maximum absolute differences between the data points and the fitting line were divided by the dynamic range to obtain the INL. To determine the charge resolution of the ToT, we used a look-up table obtained in advance to calibrate its non-linearity and offset in order to convert time widths into charge quantities. To obtain the charge resolution of the dToT, we subtracted the offset time widths derived using the fitting line from the time widths.

3.2. Gamma-ray spectra

Using both the dToT and ToT systems, we measured pulse time width spectra produced by ^{22}Na and ^{137}Cs gamma-ray sources and compared the resulting distributions with the pulse height spectra produced by a conventional pulse height analysis system (Figs. 9, 10, and 11, respectively). We used a silicon avalanche photodiode (APD) (Hamamatsu S8664-1010) coupled to a 10 mm × 10 mm × 10 mm

$Gd_3Al_2Ga_3O_{12}$ (GAGG) scintillator crystal with a decay time of 88 ns, density of 6.63 g/cm^3, and light yield of 46,000 photons/MeV [8] (Furukawa Co. Ltd.). Owing to the non-linearity of the ToT, its spectra (Fig. 10) show much distortion, especially in the low-energy region. As is seen in the figure, this non-linearity erases the back scatter peaks. Unlike the ToT spectra, the dToT spectra (Fig. 9) effectively reproduce the pulse height spectra because of their high linearity. The full energy peaks, Compton edges, and back-scatter peak are found in their proper

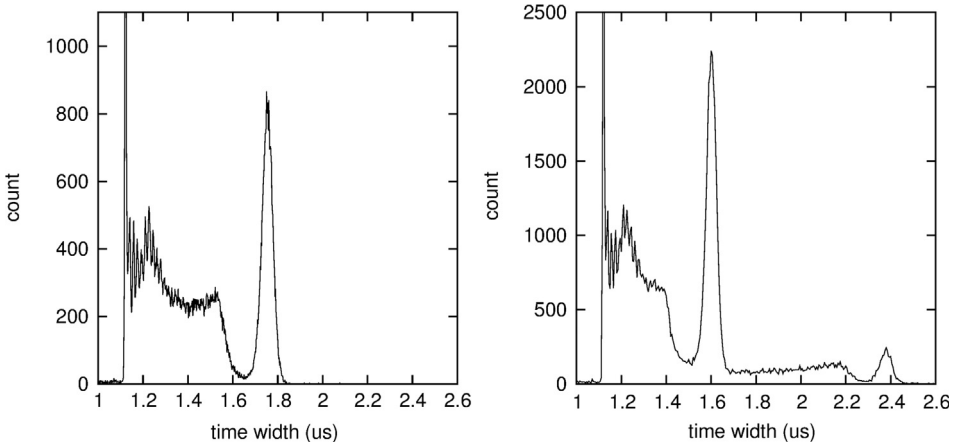

Fig. 9. dToT Spectra, Left: ^{137}Cs spectra; Right: ^{22}Na spectra.

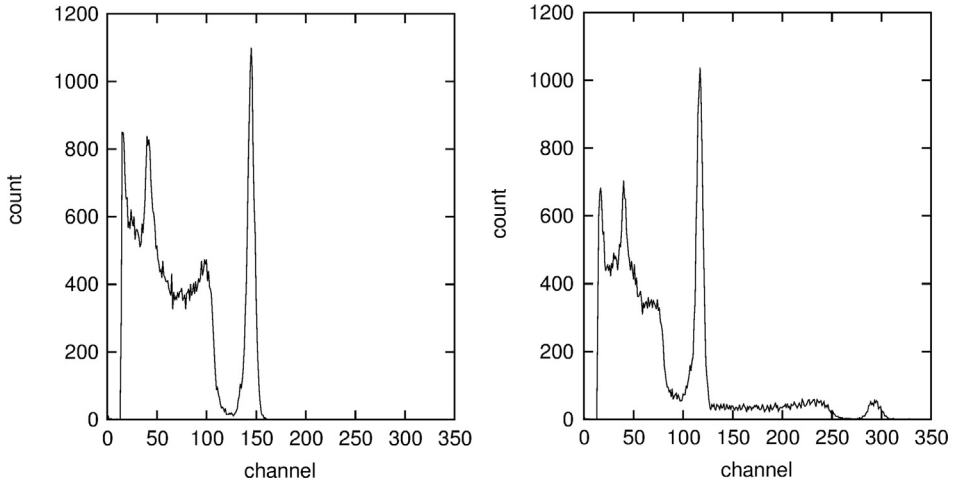

Fig. 11. Pulse height spectra Left: ^{137}Cs spectra; Right: ^{22}Na spectra.

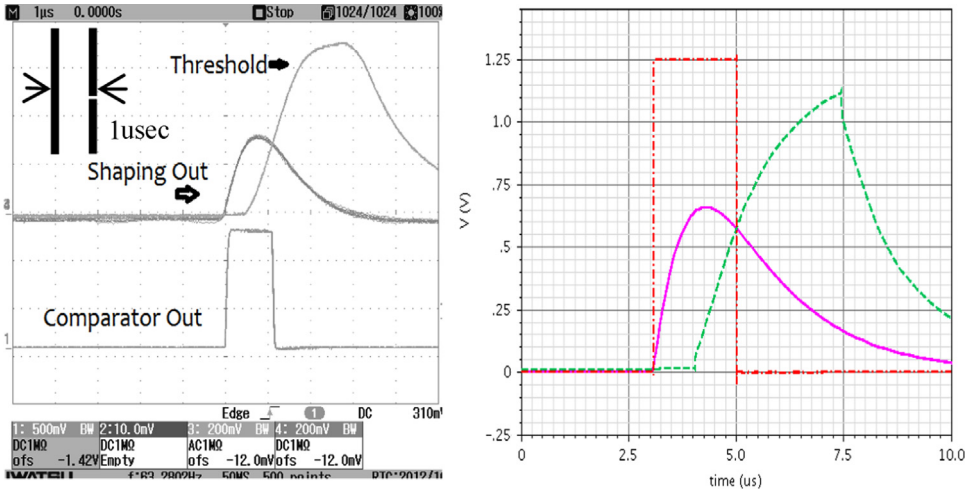

Fig. 12. Test channel output and HSPICE simulation waveforms, Solid line: Shaping output, Dashed line: Threshold, Dash-Dotted line: Comparator output.

channels without the need for any correction process. After energy calibration, the respective energy resolutions at 511 keV were 9.5% (for the dToT), 17.4% (for the ToT), and 8.3% (for the pulse height analyzer), and at 611 keV the energy resolutions were 7.5% (dToT), 15.9% (ToT), and 7.2% (pulse height analyzer). The energy peaks at 1.27 MeV were 4.5, 15.8, and 5.0% for the dToT, ToT, and pulse height analyzer, respectively.

4. ASIC

After confirming the linearity of the dToT, we designed a new application-specific integrated circuit (ASIC) using 8-channel dToT circuits. Along with HSPICE simulation waveforms, Fig. 12 shows the test channel shaping output, the threshold output, and the comparator output.

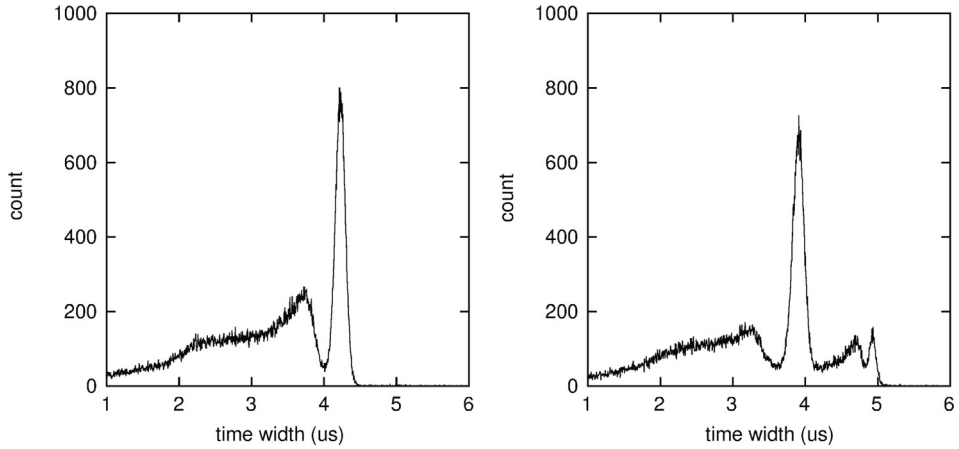

Fig. 10. ToT Spectra, Left: ^{137}Cs spectra; Right: ^{22}Na spectra.

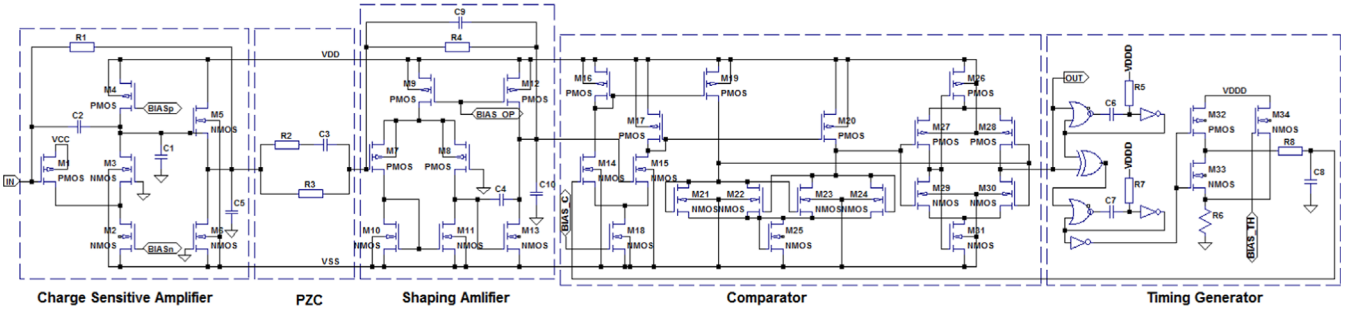

Fig. 13. Schematic of one channel of the ASIC, The European resistor symbol indicates a high resistor circuit (see Fig. 14), while the American resistor symbol indicates a normal passive resistor.

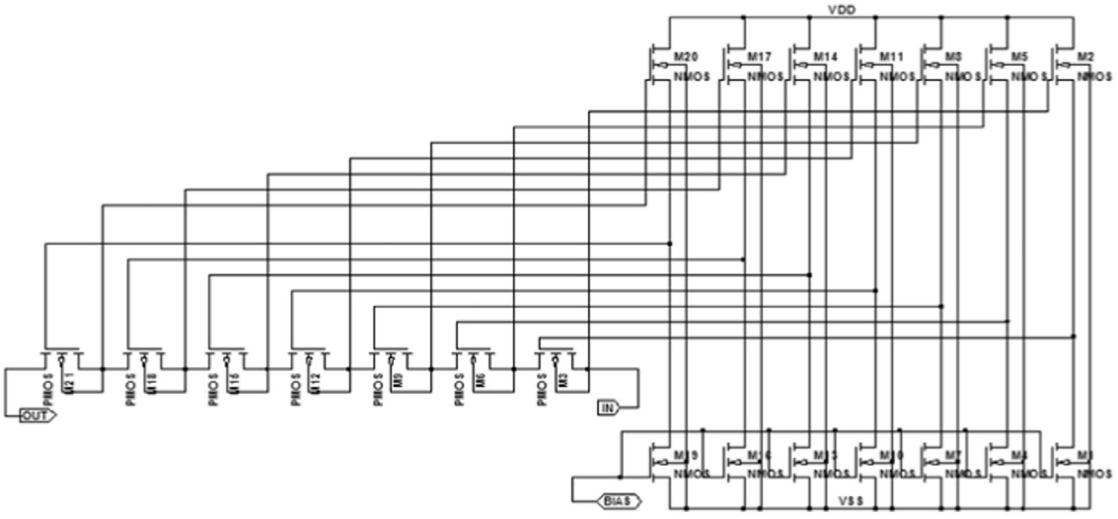

Fig. 14. CMOS resistor circuit.

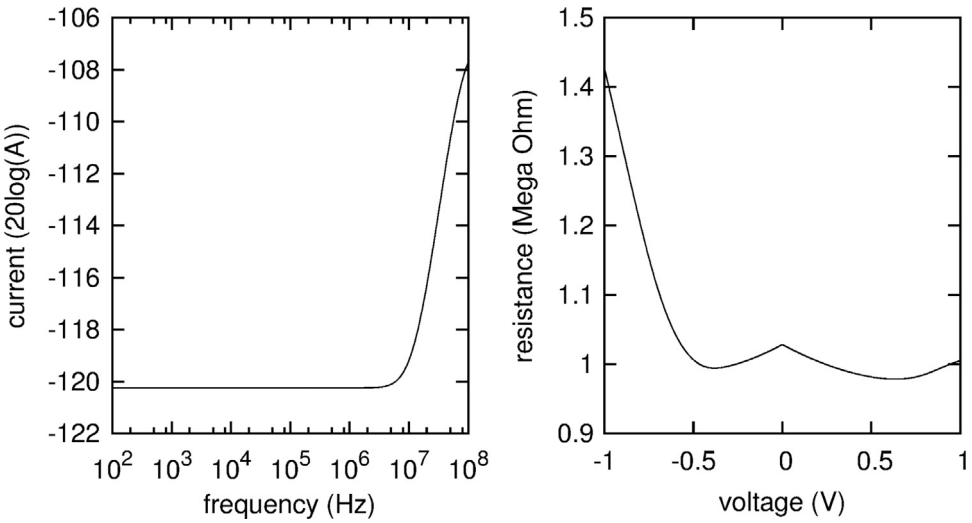

Fig. 15. Characteristics of resistor circuit, Left: AC; Right: DC characteristics.

These test channel outputs and HSPICE simulation waveforms reveal differences in the threshold waveform, particularly in the rising part, owing to the insufficiency of the RC filter frequency response and the fact that its time constant is not matched.

4.1. Circuit

All of the ASIC channels are identical, as shown schematically in Fig. 13. The timing resolution of the circuit is about 60 ns, and it has a charge sensitive amplifier (CSA), a pole-zero cancellation circuit [9], a shaper with a time constant of 1 μs, a comparator, a timing generator circuit for changing the dynamic threshold using logic circuits, and two mono-stable multi-vibrators. The CSA has a folded cascode circuit. The shaping amplifier is a normal two-stage amplifier. The feedback resistor and the resistors for shaping, pole-zero cancellation, threshold shaping and timing generator are composed of complementary metal–oxide–semiconductor (CMOS) resistor circuits that allow it to attain resistances larger than 1 MΩ without a large footprint on the Si wafer. In order to reproduce the simulation results within the circuit's dynamic range and frequency band of interest, the resistor circuit must maintain a constant resistance for an accurate Gaussian waveform. It operates within the linear region of the CMOS transistors:

$$\frac{1}{R}=\frac{dI_{DS}}{dV_{DS}}\approx \mu C_{ox}\frac{W}{L}(V_{GS}-V_{TH}) \quad (5)$$

$$V_{DS}/2 \ll V_{GS}-V_{TH} \text{ (linear region condition)} \quad (6)$$

We had to set low values of W/L and V_{GS} – V_{TH} in the level shifter circuit in order to obtain high resistance; the latter condition violates the condition in Eq. (6), making V_{DS} common for multiple resistor circuits (Fig. 14). Fig. 15 shows the DC and AC characteristics of the resistor circuit; it is seen from the figure that good response is found only in the case of forward voltage, as the drain and source terminals are inverted and the bulk terminals are terminated to the drains, which causes the level shifter circuits to supply the voltage between the drain and bulk terminals and the gate terminals. Although the resistor circuit has poor characteristics, it can perform better if the polarity of the signal is fixed, and its AC characteristics (Fig. 15) show that the circuit has a good shaping ability.

4.2. Spectra and linearity

We measured the spectra of the ^{22}Na source using a Hamamatsu 12 × 12 APD array and a 2 mm × 2 mm × 10 mm LuAG scintillator with a decay time of 20 ns, a density of 6.7 g/cm^3, and a light yield of 22,000 photons/MeV (Furukawa) (Fig. 16). A field-programmable gate array (FPGA) board (Altera DE0) was used to count the time widths of all eight channels in parallel. The spectra obtained using the dToT system show a lower energy peak at 511 keV and a higher energy peak at 1.275 MeV but, as its channel-to-channel uniformity is not high, energy calibrations were required for each channel. The average energy resolution at 511 keV is about 20%. As the dToT system has an offset in its spectra caused by its initial threshold voltage and its delay time, we calculated its energy resolution after obtaining the offset using the fitting line. By measuring the output time widths of the channels, we were able to evaluate the equivalent noise charge (ENC) of each at about 8,000 electrons full width at half-maximum (FWHM). Because of this high noise, the energy resolutions were deteriorated, with noise appearing especially in the lower part of the energy spectra. In order to obtain better energy resolution, it will be necessary to optimize the circuit design with respect to the external noise.

The linearity curve of each channel is shown in Fig. 17. As the resistor for threshold shaping does not match the target value needed to match time constants and delay time, the time constants for the delay and threshold shaping are different from that the signal shaping time constant; as a result, non-linearity appears, especially in the low energy region. As Eq. (5) shows, this resistor circuit is sensitive to MOSFET's threshold voltage variation. To obtain better linearity, a high resistance circuit that has good characteristics with respect to dynamic range and frequency and is insensitive to CMOS process variability must be designed. Nevertheless, the linearity of the dynamic time-over-threshold system seems much better than that of a normal ToT system.

5. Conclusion

In this article, we proposed a dToT circuit that uses CR-RC shaping and threshold voltage sweeping at a constant CR. The linearity of the dToT system is much better than that of a normal ToT system. Encouraged by our initial results, we designed a new multi-channel

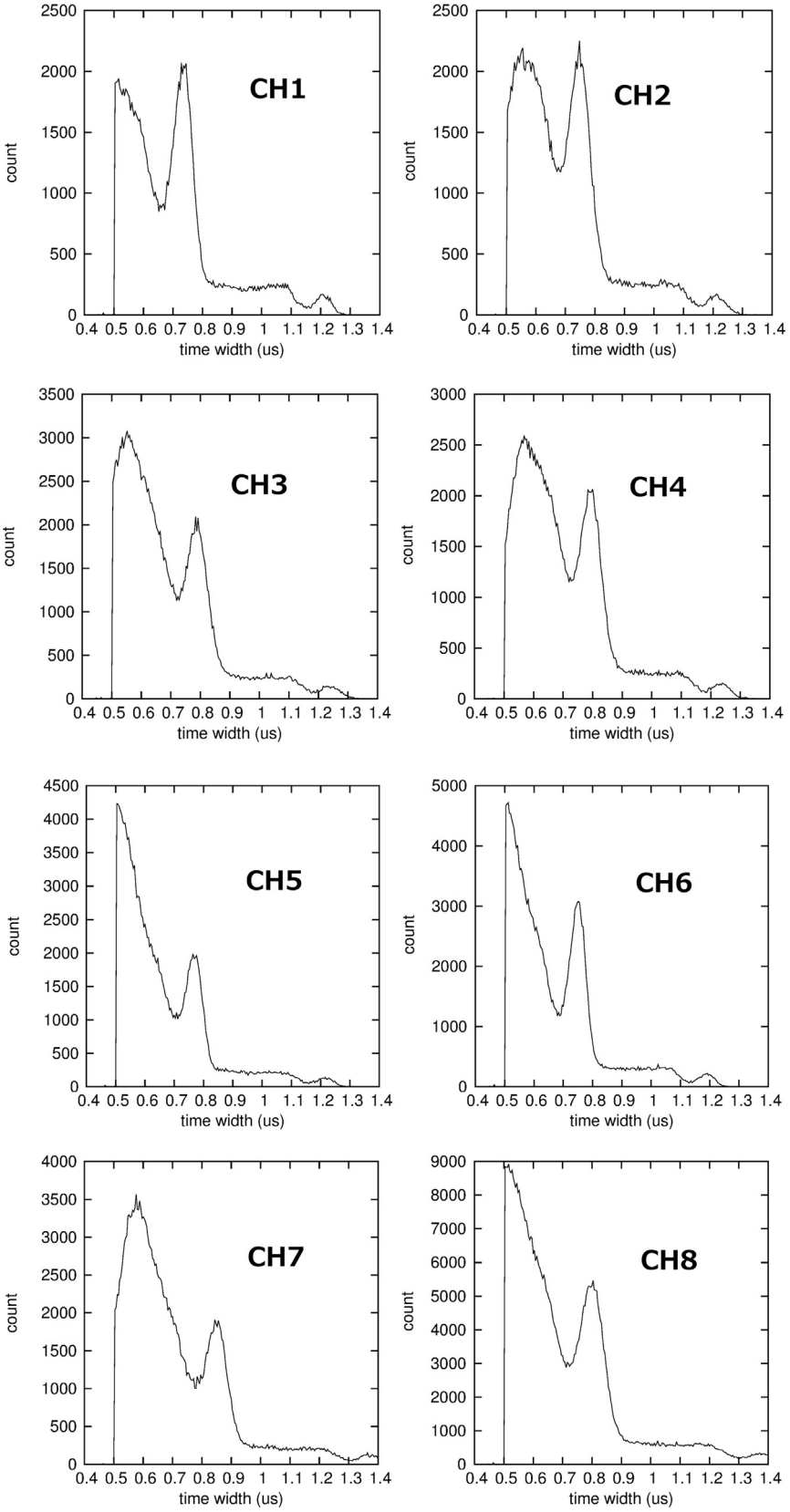

Fig. 16. ^{22}Na source spectra produced by ASIC, Energy resolutions at 511 keV are 19.9% (CH1), 20.4% (CH2), 20.0% (CH3), 20.9% (CH4), 17.5% (CH5), 16.2% (CH6), 20.3% (CH7), and 23.6% (CH8).

ASIC using the proposed dToT system to implement a pixelated APD detector. This system has a better linearity than a normal ToT system and can reproduce clear peaks from a ^{22}Na gamma-ray source. To increase linearity and reduce noise, we will have to refine the characteristics of the resistor circuit with respect to dynamic range and frequency and optimize the circuit design with respect to noise.

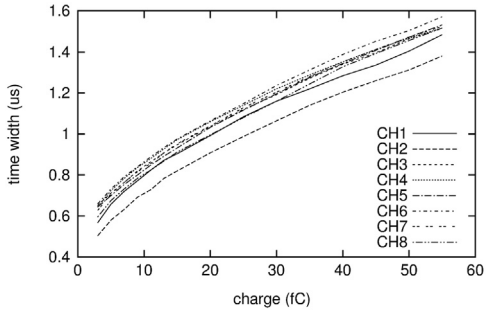

Fig. 17. Linearity curves for all eight channels, The test signal is generated from a pulse generator. INL values are 5.8%(CH1), 5.1%(CH2), 4.1%(CH3), 5.4%(CH4), 3.5%(CH5), 4.5%(CH6), 5.0%(CH7), and 4.4%(CH8).

References

[1] I. Kipnis, T. Collins, J. DeWitt, et al., A time-over-threshold machine: the readout integrated circuit for the BABAR silicon vertex tracker, IEEE T. Nucl. Sci. 3 (2002) 289–297 (NS44).

[2] F. Powolny, E. Auffray, H. Hillemanns, et al., A novel time-based readout scheme for a combined PET-CT detector using APDs, IEEE T. Nucl. Sci. 55 (2008) 2465–2474.

[3] Z. Deng, A.K. Lan, X. Sun, C. Bircher, Y. Liu, et al., Development of an eight-channel time-based readout ASIC for PET applications, IEEE T. Nucl. Sci. 57 (2011) 3212–3218.

[4] P.D. Olcotto, C.S. Levin, Pulse width modulation: a novel readout scheme for high energy photon detection, in: *Nucl. Sci. Symp. Conf. Record, 2008, NSS '08. IEEE*, Dresden, Germany, pp. 4530–4535, Oct. 19-25, 2008.

[5] C. Paul, H. Larue, M. Streun, K. Ziemons, S. Van Waasen, Fast charge to pulse width converter for monolithic PET detector, IEEE. T. Nucl. Sci. 59 (2012) 1809–1814.

[6] K. Shimazoe, H. Takahashi, S. Boxuan, T. Orita, et al., Dynamic time over threshold method, IEEE T. Nucl. Sci. 59 (2012) 3213–3217.

[7] L. Blanquart, J. Richardson, P. Denes, K. Einsweiler, et al., Analog front-end cell designed in a commercial 0.25-μm process for the ATLAS pixel detector at LHC, IEEE T. Nucl. Sci. 49 (2002) 1778–1782.

[8] K. Kamada, T. Yanagida, J. Pejchal, N. Martin, et al., Crystal growth and scintillation properties of Ce Doped $Gd_3(Ga, Al)_5O_{12}$ single crystals, IEEE T. Nucl. Sci. 59 (2012) 2112–2114.

[9] K. Tamura, T. Hiruta, H. Ikeda, et al., Development of ASICs for CdTe pixel and line sensors, IEEE T. Nucl. Sci. 52 (2005) 2023–2029.